Instrument Science Report ACS 2007-11

Calibration of ACS Ramp Filters Using the ACS Grism

A. S. Fruchter and N. Pirzkal

fruchter@stsci.edu

September 2007

Abstract

Ramp filters provide ACS users with the equivalent of tunable narrow and medium-width passband filters. Here we analyze images taken under calibration programs CAL 9671 and CAL 10742 to measure the wavelength calibration of the ACS ramp filters by observing standard stars with the ramp filters crossed with the ACS G800L grism. We find that the tested HRC ramp filters are relatively well centered on the requested wavelengths. A number of the WFC filters, however, display significant offsets from the desired central wavelength. While the WFC direct images show large image offsets (wedges) due to the crossed filters, we have attempted to remove these offsets. Our results suggest we have reduced these offsets to one pixel or less both in images taken with the ramps crossed with wideband filters and in the spatial direction of images taken with the ramps crossed with the grism. Offsets in the spectral direction of the grism images cannot be distinguished from a wavelength miscalibration. Data taken of line emission from an astrophysical source through the FR782N filter and compared to ground-based imaging suggest that this filter is well calibrated, in contrast to the result of the crossed filter observations reported here. Ray tracing simulations, deeper second order grism spectra, and further observations of astrophysical targets with known strong spectral features should be able to determine the extent to which the wavelength offsets reported here are real or an artifact of the calibration method.

1. Introduction

The Advanced Camera for Surveys (ACS) on board HST carries only a limited complement of narrow and medium band filters. Instead of a larger assortment of filters, it has several ramp filters – filters whose effective central bandwidth varies as they are rotated across the field. While these filters cannot take advantage of the full field-of-view (FOV) of the instrument at any particular wavelength (and indeed the filters themselves do not even physically cover the entire FOV of the WFC), they provide the user with great flexibility in choosing a central wavelength – an invaluable capability for many observations.

Calibration program CAL 9671 (PI Chris O'Dea) was created to measure the throughput of the ACS ramp filters at a number of settings in order to verify our understanding of their behavior on-orbit. Images of the standard star GD153 were requested with both medium band and narrow band ramp filters crossed with the G800L grism on both the High-Resolution Channel (HRC) and Wide-Field Channel (WFC). With this optical set-up, the light of the star is dispersed by the G800L grism, but then must pass through the ramp filter immediately behind the grism. The ramp only allows a relatively narrow range of wavelengths to pass on to the CCD. The central wavelength of each ramp is tunable by varying the degree of rotation of the filter wheel holding the ramp filter. More information on the use of the ramp filters can be found in the ACS Instrument Handbook.

In order to limit the amount of time required to read-out the exposures taken with the WFC, the program requested that only sub-sections of the WFC be read-out. Unfortunately, at the time this program was executed there was an as-yet unidentified error in the commanding software which caused the sub-sections to be offset from the required positions on the camera. As a result, all of the WFC images were lost. The HRC observations, however, were successful.

A preliminary reduction of the CAL 9671 observations by us showed a small but systematic offset between the requested and measured center wavelengths of the ramp filters. We therefore decided to repeat the HRC observations as part of the program to obtain the WFC calibration. Additionally, we decided to obtain direct images of the standard star not only through F606W but also with the ramp band filter crossed with F606W or another broad band filter when the ramp passband was not contained in the F606W passband. Direct F606W images are used to derive the zeropoint of a grism spectrum. By crossing the ramp filter with F606W (or another broadband filter) we hoped to replicate, and thus be able to remove, any filter wedge that was produced by crossing the grism (G800L) with the ramp. The creation of ramp filter apertures for the WFC also allowed us to be sure of both the placement of the images and a relatively efficient readout – only the quadrant of the ACS in the field-of-view of a particular ramp is read out. In this ISR, we report on these

observations and the results of our analysis.

2. The Data and Analysis

In CAL 9761, images of the standard star GD153 were obtained with the HRC in several filter settings. The narrow band ramp, FR656N, was crossed with the G800L grism and set at central wavelengths of 6366, 6559 and 6752 $\AA$. GD153 was also observed through the medium band ramp, F914M, with settings of 7884, 8512, 9140, 9768 and 10396 $\AA$. Additionally, observations were taken with only the G800L (grism), the F606W or F775W filters in place. In Table 1, we list all of the HRC exposures from CAL 9761, along with filters used, the wavelength setting of the linear ramp filter (where appropriate) and the exposure time of each image.

Table 1: CAL 9671 HRC Observations

Exposure	Aperture	Filter1	Filter 2	LRF ($\AA$)	Exp. Time (s)
j8iv01p8q	HRC	G800L	FR656N	6366	60
j8iv01p9q	HRC	G800L	FR656N	6559	60
j8iv01paq	HRC	G800L	FR656N	6752	60
j8iv01pbq	HRC	F775W	CLEAR2S		10
j8iv01pcq	HRC	F606W	CLEAR2S		180
j8iv01peq	HRC	G800L	CLEAR2S		60
j8iv01pfq	HRC	G800L	FR914M	7884	60
j8iv01pgq	HRC	G800L	FR914M	8512	60
j8iv01phq	HRC	G800L	FR914M	9140	60
j8iv01piq	HRC	G800L	FR914M	9768	60

For CAL 10742, scheduling constraints required us to use another standard star, AGK+81d266. We observed the star with both the HRC and the WFC. With the HRC, we observed using both the FR656N and FR914M ramp filters as in CAL 9761. However, in addition to direct images through a single filter, we also obtained images of the star using the appropriate ramp filter crossed with a broadband filter. In the case of FR656N, the ramp was crossed with F606W, which is the standard reference filter for setting the zeropoint of the wavelength scale of a grism observation. However, as the passband of

FR914M is not contained in the passband of F606W, we crossed FR914M with F850LP to obtain a direct stellar image for the wavelength zeropoint. A complete list of the exposures for the HRC component of CAL 10742 can be found in Table 2.

Table 2: CAL 10742 HRC Observations

Exposure	Aperture	Filter1	Filter 2	LRF ($\AA$)	Exp. Time (s)
j9mo04tdq	HRC	F606W	CLEAR2S		0.5
j9mo04teq	HRC	CLEAR1S	FR656N	6560	2
j9mo04tfq	HRC	F606W	FR656N	6560	5
j9mo04tgq	HRC	G800L	CLEAR2S		5
j9mo04thq	HRC	G800L	FR656N	6300	20
j9mo04tiq	HRC	G800L	FR656N	6450	20
j9mo04tjq	HRC	G800L	FR656N	6600	20
j9mo04tkq	HRC	G800L	FR656N	6780	20
j9mo04tlq	HRC	CLEAR1S	FR914M	9000	2
j9mo04tmq	HRC	F850LP	FR914M	9000	5
j9mo04tnq	HRC	G800L	CLEAR2S		5
j9mo04toq	HRC	G800L	FR914M	7800	20
j9mo04tpq	HRC	G800L	FR914M	8500	20
j9mo04tqq	HRC	G800L	FR914M	9200	20
j9mo04trq	HRC	G800L	FR914M	9900	20

Similarly, for the WFC observations of CAL 10742, the direct image that would be used to derive the wavelength zeropoint of the grism spectrum of a ramp filter was derived by crossing the filter with F606W if the ramp was contained in the F606W passband. Otherwise, another broadband filter was substituted for F606W. Thus F850LP was used for FR914M, FR853N and FR931N, while F775W was used with FR782N. A complete list of the WFC exposures can be found in Table 3.

The images were passed through the standard ACS data pipeline, and the spectra were extracted using the aXe software package (Pirzkal et al., 2003). For CAL 9671, the F606W direct image was used to set the wavelength zeropoint. For CAL 10742, the appropriate crossed filter direct image was used. In order to convert the measured fluxes to transmission, the measured flux of the stellar spectrum was divided by the cataloged spectra of the standards using a local black body approximation across each filter. In

Table 3: CAL 10742 WFC Observations

Exposure	Aperture	Filter1	Filter 2	LRF ($\AA$)	Exp. Time (s)
j9mo01gjq	WFC1-MRAMPQ	F606W	CLEAR2L		0.5
j9mo01gkq	WFC1-MRAMPQ	F606W	FR656N	6560	3
j9mo01glq	WFC1-MRAMPQ	G800L	FR656N	6500	8
j9mo01gmq	WFC1-MRAMPQ	G800L	FR656N	6700	8
j9mo01goq	WFC1-MRAMPQ	G800L	FR914M	8200	8
j9mo01gpq	WFC1-MRAMPQ	G800L	FR914M	9000	8
j9mo01gqq	WFC1-MRAMPQ	G800L	FR914M	10000	8
j9mo01grq	WFC1-MRAMPQ	F850LP	FR914M	9200	1
j9mo02siq	WFC1-IRAMPQ	F606W	CLEAR2L		0.5
j9mo02sjq	WFC1-IRAMPQ	F606W	FR647M	6200	2
j9mo02skq	WFC1-IRAMPQ	G800L	FR647M	5900	8
j9mo02slq	WFC1-IRAMPQ	G800L	FR647M	6500	8
j9mo02snq	WFC1-IRAMPQ	G800L	FR647M	7100	8
j9mo02soq	WFC1-IRAMPQ	F850LP	FR853N	8650	2
j9mo02spq	WFC1-IRAMPQ	G800L	FR853N	8400	8
j9mo02sqq	WFC1-IRAMPQ	G800L	FR853N	8700	8
j9mo03liq	WFC2-ORAMPQ	F606W	CLEAR2L		0.5
j9mo03ljq	WFC2-ORAMPQ	F850LP	FR931N	9300	1
j9mo03lkq	WFC2-ORAMPQ	G800L	FR931N	9000	8
j9mo03llq	WFC2-ORAMPQ	G800L	FR931N	9300	8
j9mo03lnq	WFC2-ORAMPQ	G800L	FR931N	9600	8
j9mo03loq	WFC2-ORAMPQ	F775W	FR782N	7820	2
j9mo03lpq	WFC2-ORAMPQ	G800L	FR782N	7550	6
j9mo03lqq	WFC2-ORAMPQ	G800L	FR782N	8050	6

effect, the black body provides a smooth interpolation which matches the cataloged spectra to a few percent throughout all regions of interest. For GD153 we used the cataloged spectral values of Bohlin, Colina and Finley 1995, and for AGK+81d266, we used the values of Turnshek et al. 1990. Numerical tables and graphs of these spectra can be downloaded from http://stsdas.stsci.edu/ETCDEV/ACS/stis_models.html. For a more detailed discussion of the stellar spectra used in the calibration of HST filters see

http://www.stsci.edu/hst/observatory/cdbs/calspec.html.

3. Results

Figures 1 and 2 show the measured transmission of the FR656N and FR914M ramp filters under program CAL 9761. In this program no filter cross was used to obtain the direct stellar image to set the spectral zeropoint. As in standard grism observations a direct F606W image was used. Note that in the FR656N graph, all of the wavelength settings are slightly offset from the peak and mean wavelengths of the filters by about one pixel or $\sim 25\mathring{A}$ each. This offset is small compared to the full-width at half maximum (FWHM) of the ramp, but it appears to be a systematic shift. Using the FR914M filter, shown in Figure 2, there is also a small systematic shift of the wavelength setting from the centroid of the passband, but this tends to place the requested wavelength near the peak transmission of the filter, and this may be preferable to a placement on the centroid. The apparent offset for the final setting of FR914M, 10396 $\mathring{A}$, is caused by the cutoff of the extraction by the aXe software, which avoids the region where the blue part of the second order spectrum overlaps the red end of the first order spectrum. The long wavelength end of the passband is thus missing from the extraction.

In Figures 3 and 4 we show the derived passbands for the same filters, at somewhat different wavelength setting under program CAL 10742, where we have used a filter cross with the requested ramp to obtain the direct image used for the wavelength zeropoint. The requested setting of the FR656N filter now more closely matches the peak of the transmission in these filters, but the change is not dramatic. This is to be expected on two counts: the original CAL 9671 images showed relatively good reproduction of the wavelength settings and our measurements of the difference in position between the standard star in the F606W image and the crossed filter images on the HRC show minimal filter wedges.

In Table 4 we present the measured filter wedges for observations in CAL 10742. The measured wedges for the HRC are small – of order one pixel in the case of FR914M and even less for FR656N. (The direction of dispersion on the HRC is roughly 45° off of the axes, in the direction positive x and negative y. On the WFC the axis of dispersion is roughly parallel to the x-axis.) Larger wedges are seen in the case of the WFC. The optics of the HRC and the WFC are, however, different. The beam of the WFC converges more rapidly – it is for this reason that the HRC can be used without any filter in place, while the WFC is badly out of focus without a filter. Similarly, the FWHM of the HRC PSF only grows from about 2 to 2.3 pixels when a second filter is inserted in the beam. When a second filter

is inserted in the path of the WFC, the PSF goes from under 2 pixels to approximately 5 pixels. Nonetheless, on any given WFC aperture the filter wedges of different filter pairs agree to about one pixel. Both the HRC and WFC were designed to have differential wedges (with single filters) of about one pixel or less, and we are no doubt seeing the result of that design here. Thus, our method of using a crossed filter pair to determine the filter wedge of the grism should work to about 1 pixel. Our examination of the extracted spectral images obtained by aXe further supports this contention. We find that the dispersed images typically agree with the predicted position based on the cross-filter stellar image with an r.m.s. of less than one pixel in the spatial direction of the extraction. Our procedure should then also allow us to determine the wavelength calibration of the WFC.

Table 4: Observed Filter Wedges

Exposure	Aperture	Filter1	Filter 2	x-wedge (pix)	y-wedge (pix)
j9mo04tdq	HRC	F606W	CLEAR2S	0.	0.
j9mo04tfq	HRC	F606W	FR656N	-0.4	-0.2
j9mo04tlq	HRC	CLEAR1S	FR914M	-1.5	0.7
j9mo04tmq	HRC	F850LP	FR914M	-1.3	0.95
j9mo01gjq	WFC1-MRAMPQ	F606W	CLEAR2L	0.	0.
j9mo01gkq	WFC1-MRAMPQ	F606W	FR656N	-2.6	-5.0
j9mo01grq	WFC1-MRAMPQ	F850LP	FR914M	-3.8	-3.6
j9mo02siq	WFC1-IRAMPQ	F606W	CLEAR2L	0.	0.
j9mo02sjq	WFC1-IRAMPQ	F606W	FR647M	3.8	-5.5
j9mo02soq	WFC1-IRAMPQ	F850LP	FR853N	4.5	-4.7
j9mo03liq	WFC2-ORAMPQ	F606W	CLEAR2L	0.	0.
j9mo03ljq	WFC2-ORAMPQ	F850LP	FR931N	-3.9	3.0
j9mo03loq	WFC2-ORAMPQ	F775W	FR782N	-3.8	3.9

As can be seen in Figure 5, the requested wavelengths on the FR656N filter agree on the WFC relatively well with the peak wavelengths observed – the requested wavelengths are within two pixels (80$\mathring{A}$) of the peak. However, in comparison to Figure 3, the filter appears both wider and less efficient than one might expect. This is due to the defocusing caused by the filter crossing. As noted earlier, the PSF in the WFC with two filters crossed has a FWHM of 5 pixels, and is far from Gaussian. The spectrum is convolved with this enlarged PSF, both in the spatial and wavelength directions. We therefore would not

expect the measured peak height or width of the filter to be conserved – but would expect the total integrated flux to be comparable to that found in Figure 3. This interpretation is supported by Figures 6, where the transmission of the WFC FR914M filter is found at least as high as that measured in the HRC (Figure 2). The intrinsic width of the FR914M filter is greater than that of the broadened PSF, and therefore the peak transmission is not significantly compromised.

However, another trend may be discerned in Figure 6, which is also present in many of the remaining observations using the WFC. There is a significant offset between the desired and measured central wavelength of the ramp filter. While the wavelength calibration of the bluest setting of the FR647M filter agrees well with the data, as one goes to the red there appears to be a shift off of the center of the passband. As can be seen in Figures 7 through 10, the remaining filters all show significant offsets from the requested wavelengths.

Each ramp filter illuminates only a fraction of the detector. (see Figure 11 for the locations of the various apertures on the chips). Some of the ramps can illuminate only part of a single quadrant of the detector. Some can be placed on opposing quadrants of WFC1 and WFC2. Special apertures have been created to speed up the read-out of the ramps. These apertures read out the appropriate 2048x2046 (near) quadrant from the two 2048x4096 detectors. In order to calibrate the data these apertures were placed by us into full 2x2048x4096 fits files, so that the standard aXe calibration files could be used. A possible source of difficulties could then be that we somehow erroneously placed the quandrant into the wrong section of the full image, or that the section is incorrectly read out. We have therefore carefully checked that the WCS of the original images gives an accurate location of the calibration star, and that the quadrants have been placed correctly in the larger holder image file. We do not believe, therefore, that an incorrect alignment of the image could be responsible for the observed wavelength offsets.

4. Discussion

Without any arc lamps or similar spectral line sources, the ACS has no internal means for the wavelength calibration of its ramp filters. Here we have attempted to check the wavelength calibration by crossing the G800L grism with the ramps while observing standard stars. Crossing filters adds an additional filter path, and thus a filter wedge. We have shown this wedge to be small in the HRC, and have found the wavelength calibration of the HRC to be good – though only two filters, FR656N and FR914M were tested. While FR656N also behaved well on the WFC, redder filter – those beyond about 7500$\mathring{A}$, generally gave poorer results.

We have found, however, that the spatial wedge produced by introducing a second filter is relatively stable, even in the WFC, and thus should be removed by our use of crossed filters to obtain the direct image for the zero point setting of the grism spectrum. Two possibilities therefore seem to remain: some of the WFC ramp filters are indeed miscalibrated or we are observing an artifact possibly caused by the varying angle of incidence produced by the G800L grism. The grism sits in front of the ramp filters. Therefore, the light is dispersed before it passes through the ramps. The red light experiences the greatest deflection before incidence on the ramp filters, and thus is farthest from its expected angle of incidence. A change in angle of incidence can be expected to produce a change in central wavelength of an interference filter. However, it is less clear in this case why the relatively parallel beam of the HRC does not also experience this effect. Furthermore, while most of the WFC filters appear to show a shift to the red of the desired wavelength, two, FR782N and FR931N (Figures 9 and 10) show a shift to the blue. Interestingly these are the only two filters that use apertures on the WFC2 chip. All of the other WFC filters use either the MRAMP or RAMP apertures on WFC1. We have attempted to find a reason for this apparent correlation. An obvious source of error could be the incorrect placement of the quadrant into the full image before extraction of the spectra. However, as described above, we have carefully checked the quadrant placement and have not found a problem.

Given that the offsets we are seeing could be a result of the calibration method itself, we did a search of archival observations using the ramp filters. One observation looked as though it could provide a direct test of the ramp filter center wavelengths. Heckman et al. (GO 10920) used the FR782N filte to observe Hα emission from nearby Lyman-break galaxies. Given the large offset in central wavelength seen in Figure 7, we might expect these observations to find little or no emission. However, Overzier and Heckman (personal communication) have reported to us that the observed emission flux matches that seen by the ground to about 20%. This, they believe, is within the accuracy of their continuum subtraction. Thus the one observation of an external source that we have been able to use as a test finds no wavelength offset.

Several methods might be used to better determine the source of the calibration errors seen by us. Ray tracing software may be able to determine whether the deflection caused by the grism is sufficient to produce the wavelength shifts seen here. Indeed, ray tracing software may be able to predict the observed shift to an accuracy sufficient to use these data for calibration of the ramps. Additionally, deeper exposures with significant signal-to-noise ratios on the second order spectrum would provide a strong test of any ray tracing prediction, because the second order spectrum is greatly deflected from the original angle of incidence. Further observations of astronomical sources with strong spectral features can provide an additional verification of line centers of the ramps. In any event,

the apparent agreement of ground-based observation with at least one of the suspect ramps suggests that we may be detecting an internal calibration issue, rather than a cause of concern for our observers.

Acknowledgements

We would like to the Jeremy Walsh Adam Riess and Marco Sirianni for helpful conversations, and Ralph Bohlin, Ron Gilliland and Marco Sirianni for their careful reading of this ISR and many useful comments.

References

Bohlin, R.C., Colina, L., Finley, D.S. 1995, AJ, 110, 1316.

Pirzkal, N., Pasquali, A., Hook, R.N., Walsh, R., Albrecht, R. 2003, ASP Conf. Ser., 295, 485.

Turnshek, D.A. et al. 1990, AJ, 99, 1234.

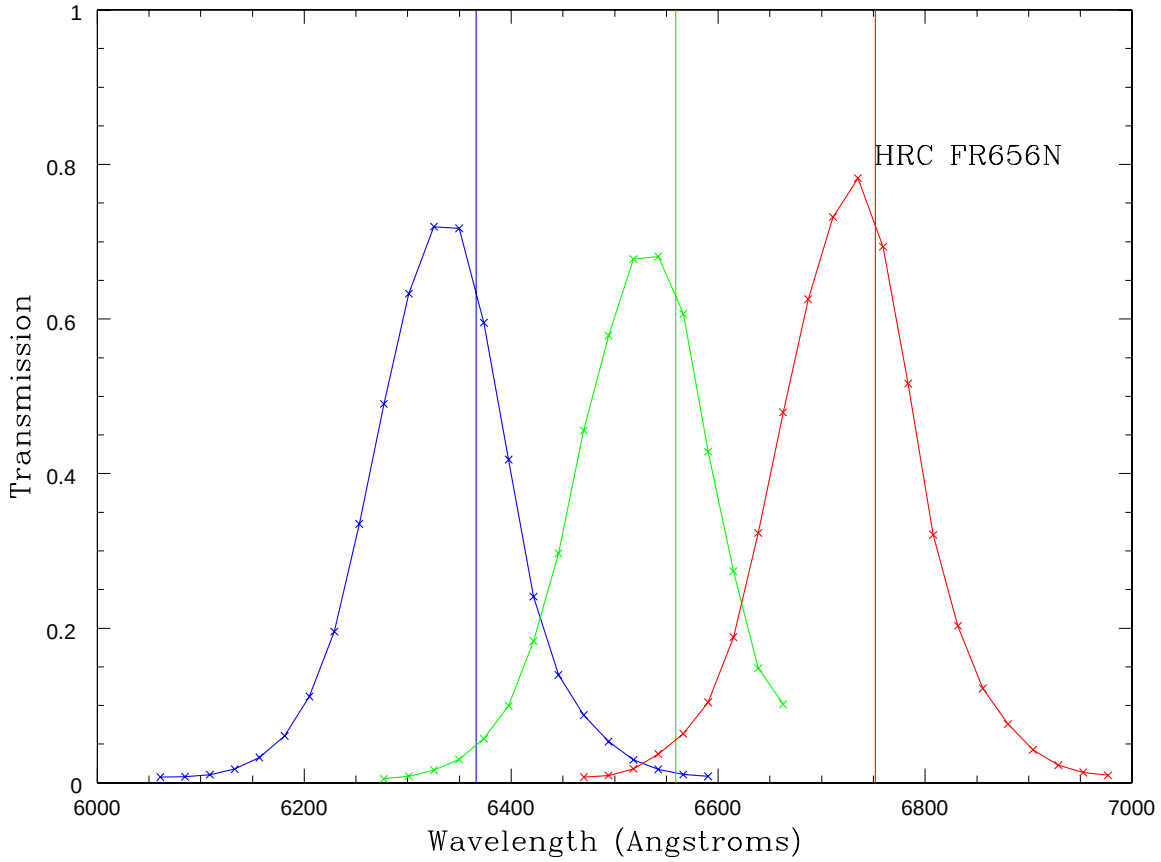

Fig. 1.— Plots of the measured transmission of the ramp filter FR656N on the HRC, set at three central wavelengths: 6366, 6559 and 6752 $\mathring{A}$. These wavelengths are shown by the vertical lines. The long-wavelength end of the spectrum of the second setting, with expected central wavelength 6559 $\mathring{A}$, was corrupted by a cosmic-ray, and is not shown. These observations were taken as part of CAL 9671.

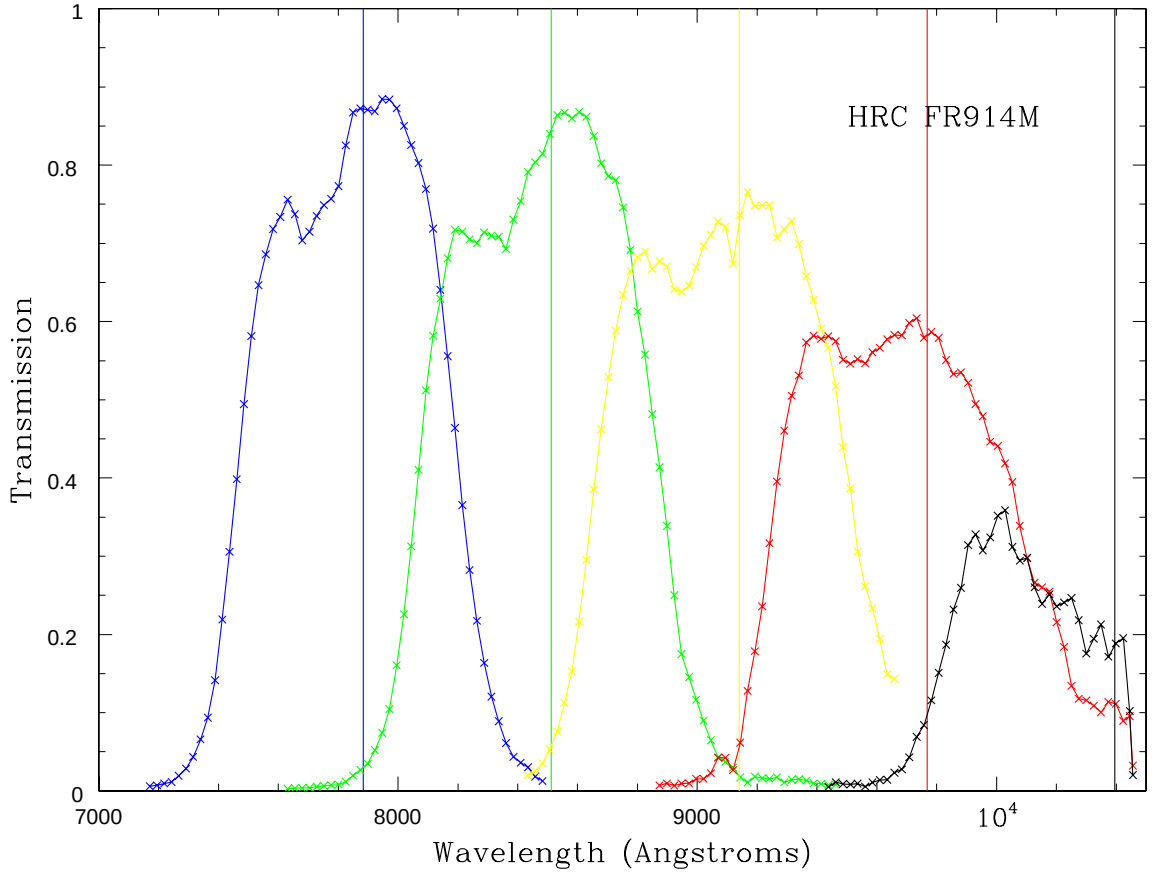

Fig. 2.— Plots of the measured transmission of the ramp filter FR914M on the HRC, set at five central wavelengths: 7884, 8512, 9140, 9768 and 10396 $\mathring{A}$. These wavelengths are shown by the vertical lines. The long-wavelength end of the spectrum of the third setting, with expected central wavelength 9140 $\mathring{A}$, was corrupted by a cosmic-ray, and is not shown. These observations were taken as part of CAL 9671.

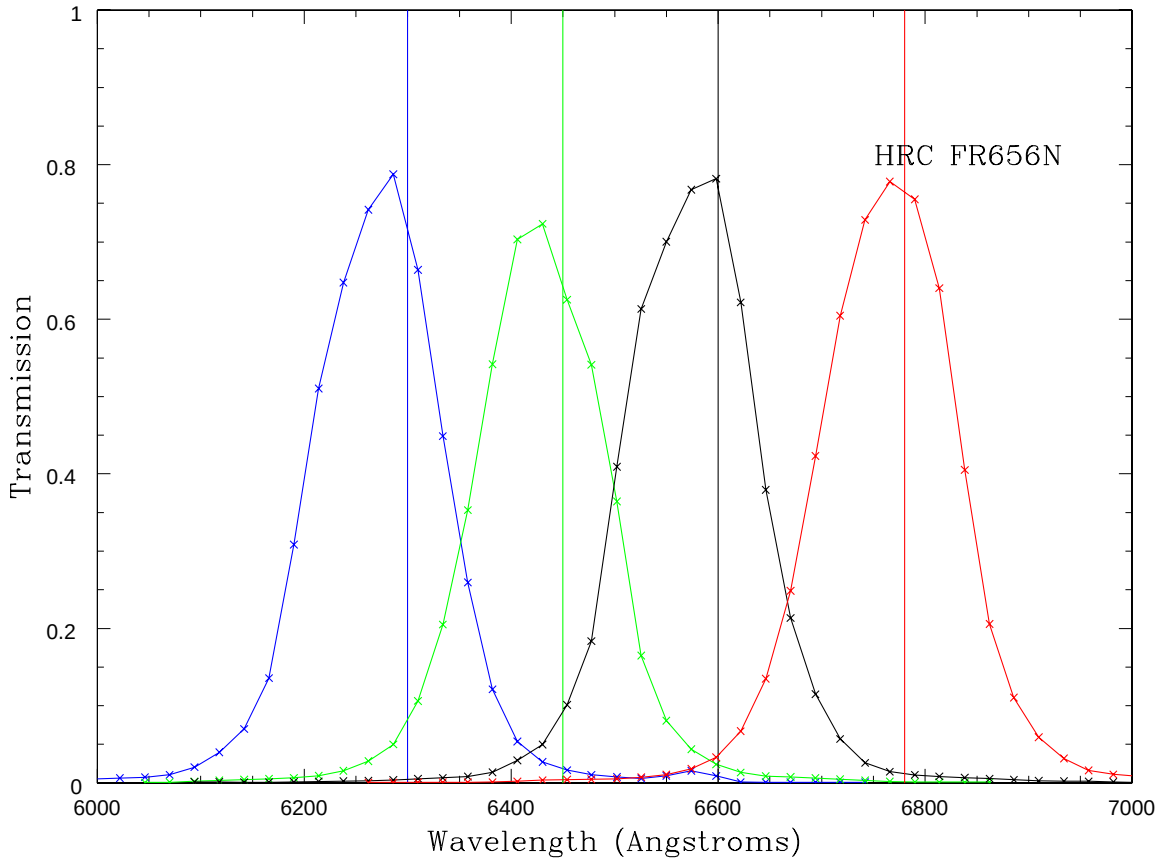

Fig. 3.— Plots of the measured transmission of the ramp filter FR656N on the HRC, set at central wavelengths: 6300, 6450, 6600 and 6780 $\mathring{A}$, shown by the vertical lines. These observations were taken as part of CAL 10742.

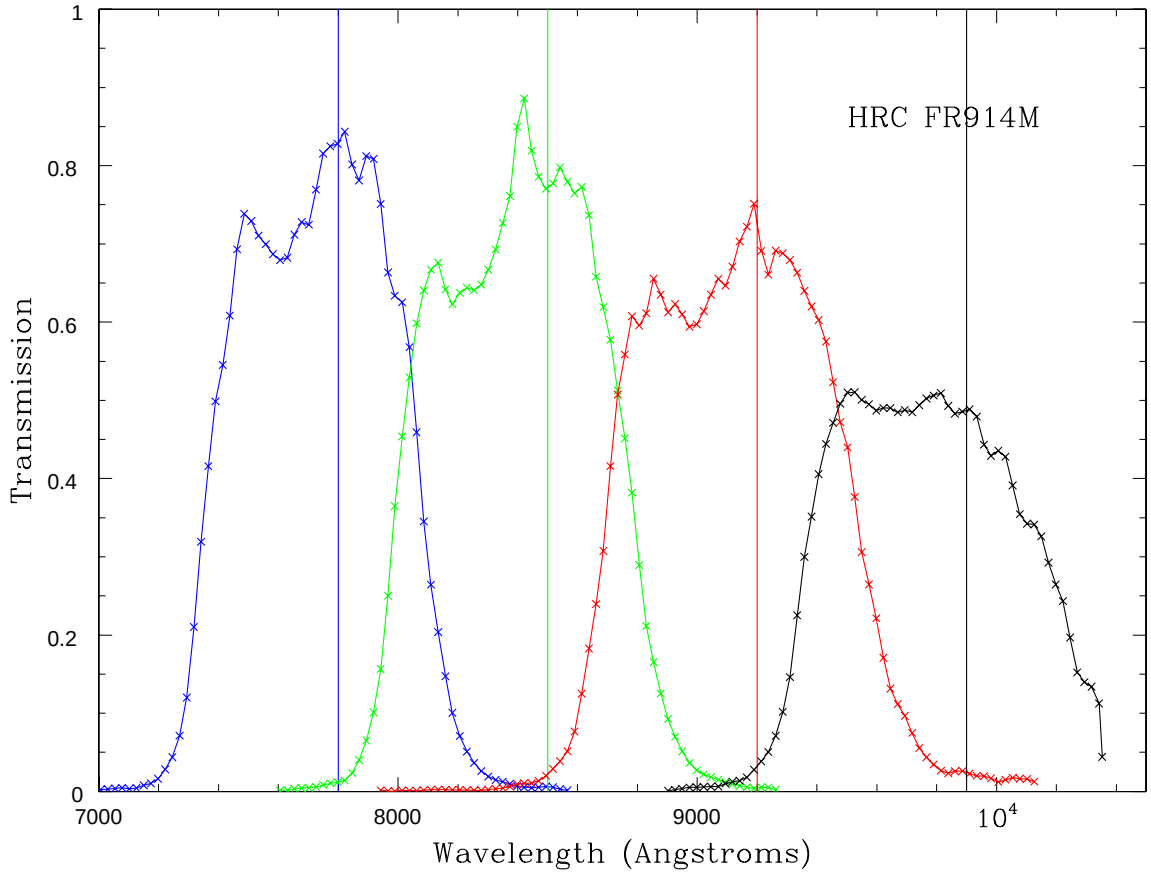

Fig. 4.— Plots of the measured transmission of the ramp filter FR914M on the HRC, set at four central wavelengths: 7800, 8500, 9200 and 9900 $\mathring{A}$, shown by the vertical lines. These observations were taken as part of CAL 10742.

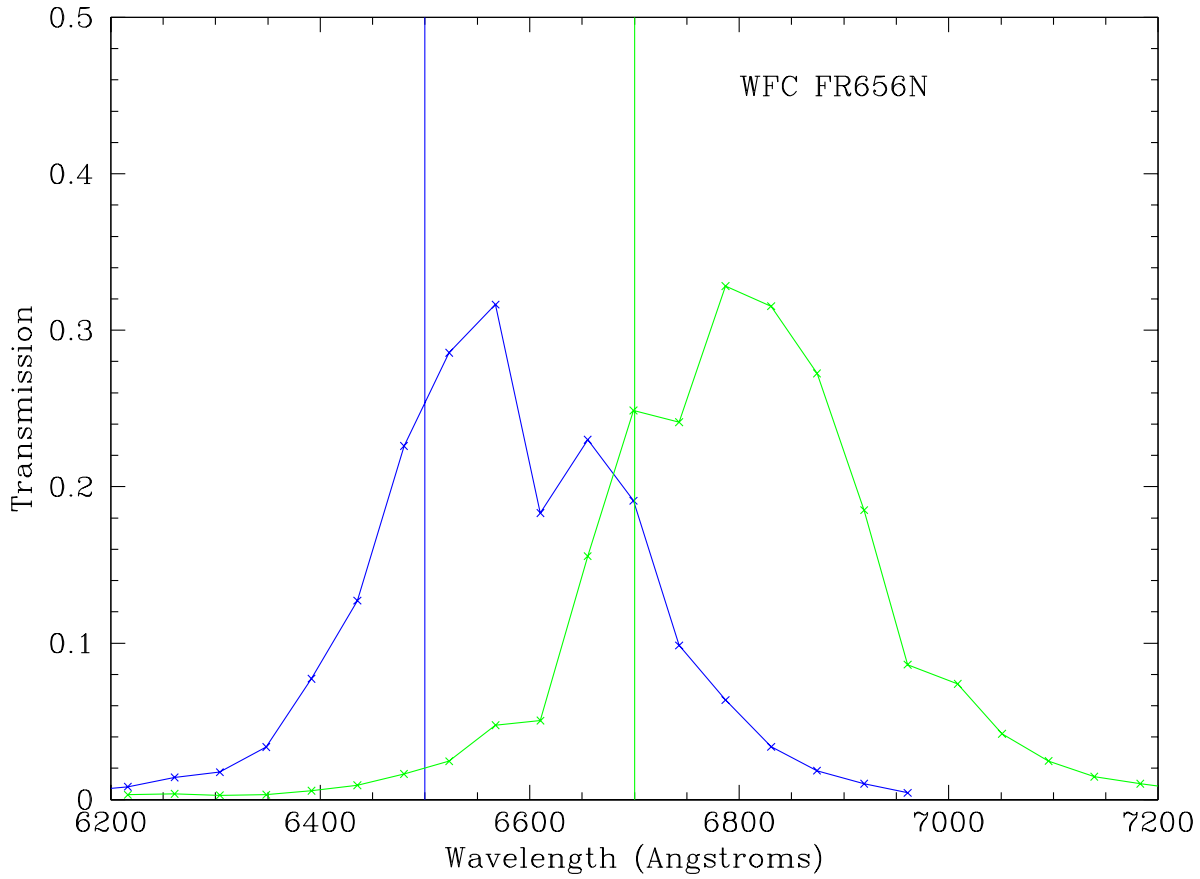

Fig. 5.— Plots of the measured transmission of the ramp filter FR656N on the WFC, set at two central wavelengths: 6500 and 6700 $\mathring{A}$, shown by the vertical lines.

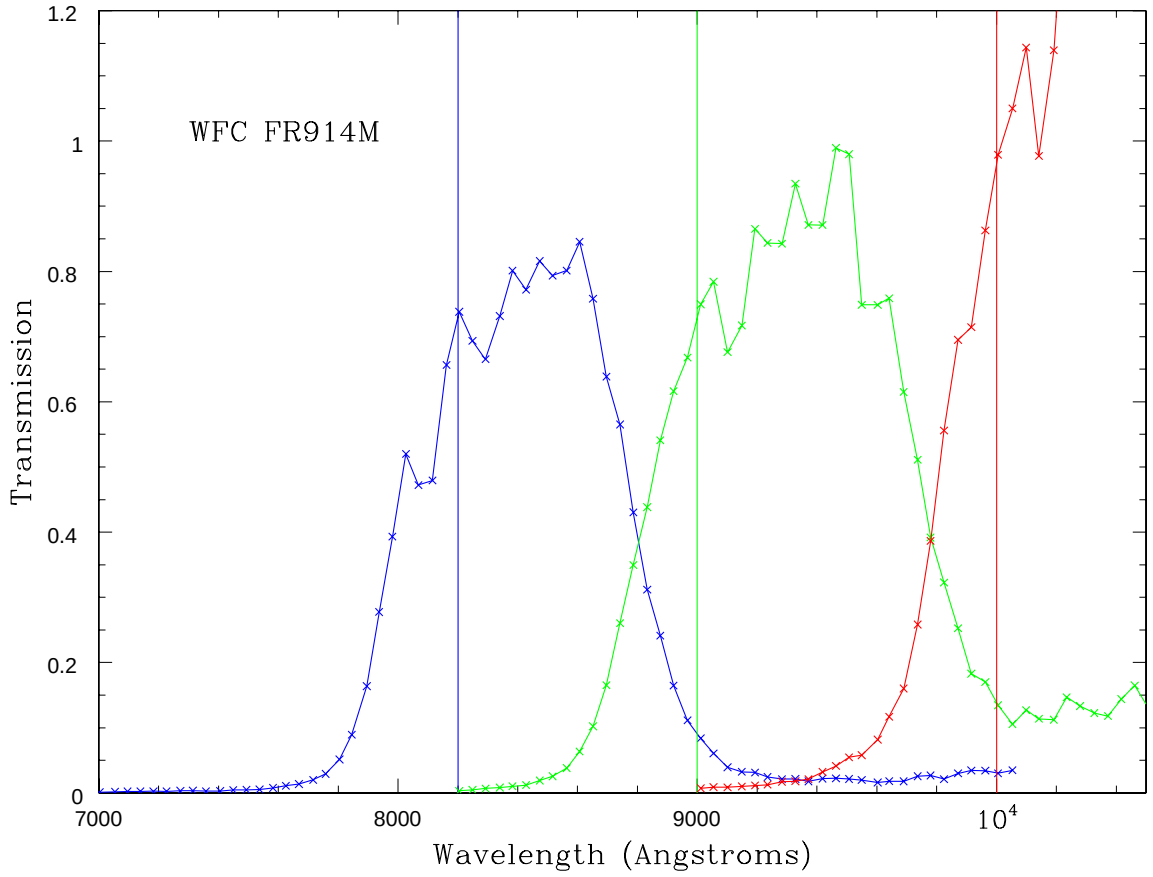

Fig. 6.— Plots of the measured transmission of the ramp filter FR914M on the WFC, set at three central wavelengths: 8200, 9000 and 10,000 $\mathring{A}$. The transmission of greater than 100% for the setting of $10,000\mathring{A}$ is most likely caused by an extrapolation of the stellar spectrum beyond $9200\mathring{A}$, combined with a poor understanding of the flat-field of the grism below $10,000\mathring{A}$.

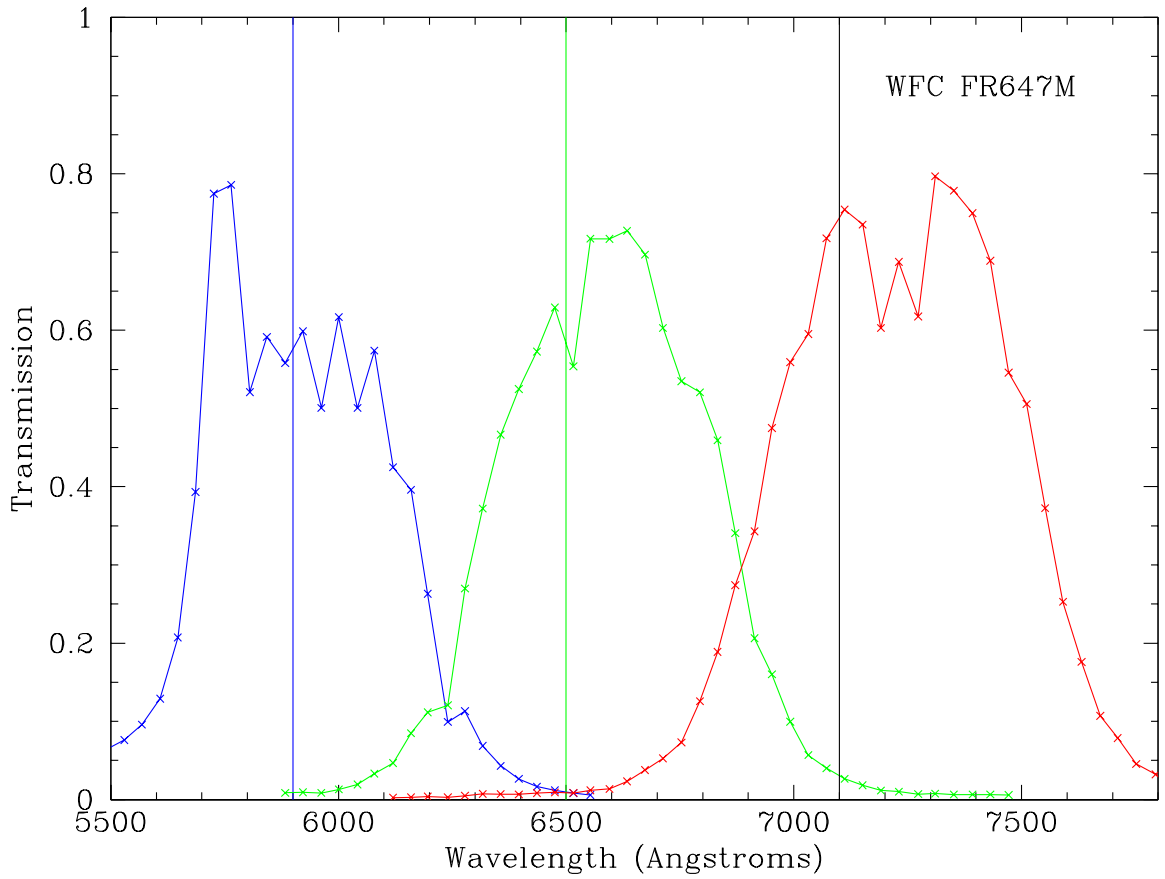

Fig. 7.— Plots of the measured transmission of the ramp filter FR647M on the WFC, set at three central wavelengths: 5900, 6500 and 7100 $\mathring{A}$, shown by the vertical lines.

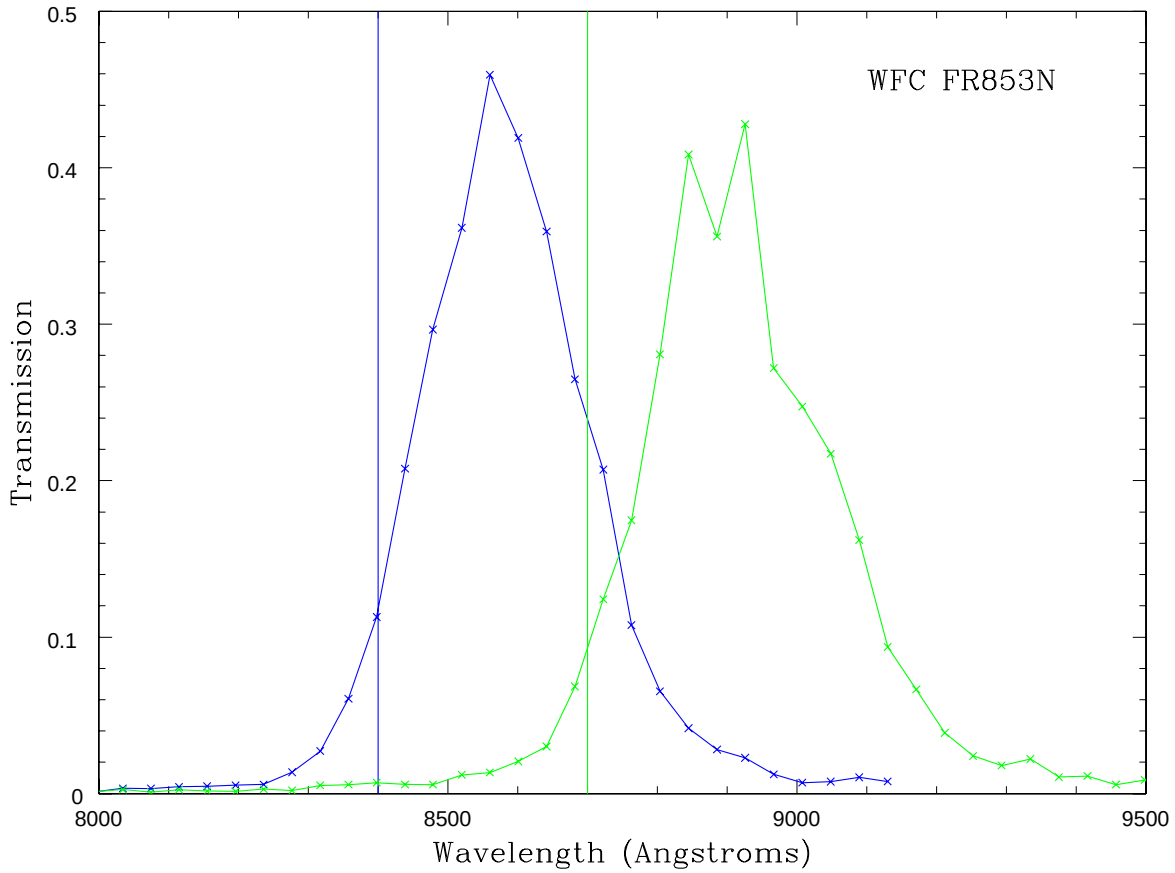

Fig. 8.— Plots of the measured transmission of the ramp filter FR853N on the WFC, set at two central wavelengths: 8400 and 8700 $\mathring{A}$.

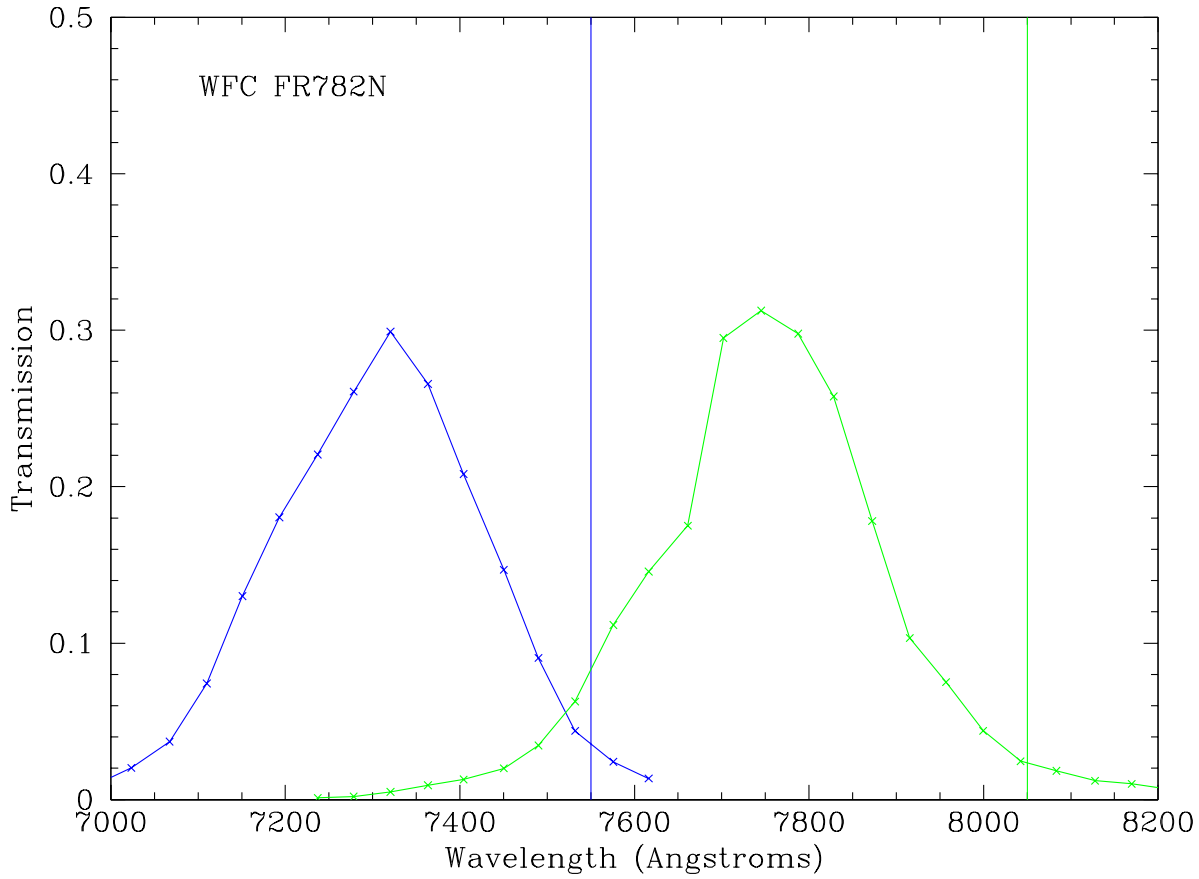

Fig. 9.— Plots of the measured transmission of the ramp filter FR782N on the WFC, set at two central wavelengths: 7550 and 8050 $\mathring{A}$.

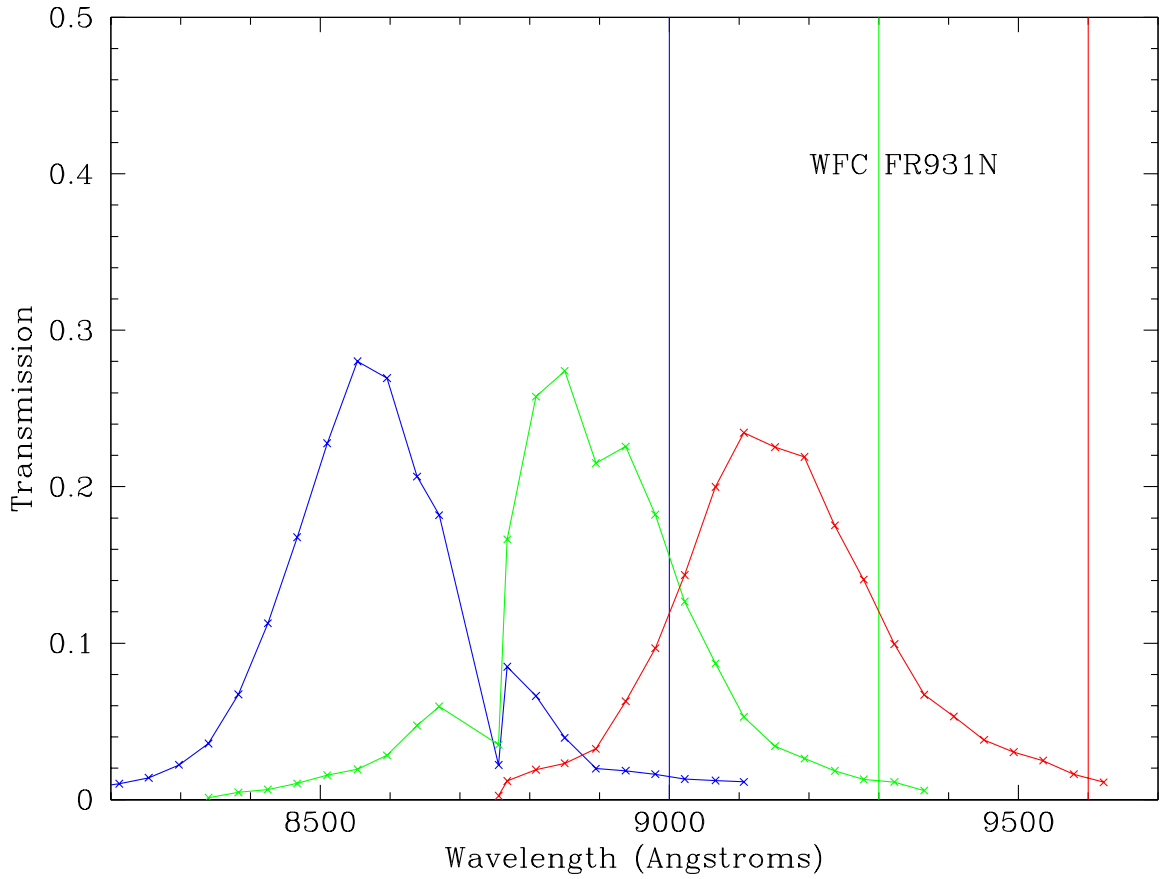

Fig. 10.— Plots of the measured transmission of the ramp filter F931N on the WFC, set at three central wavelengths: 9000, 9300 and 9600 $\mathring{A}$.

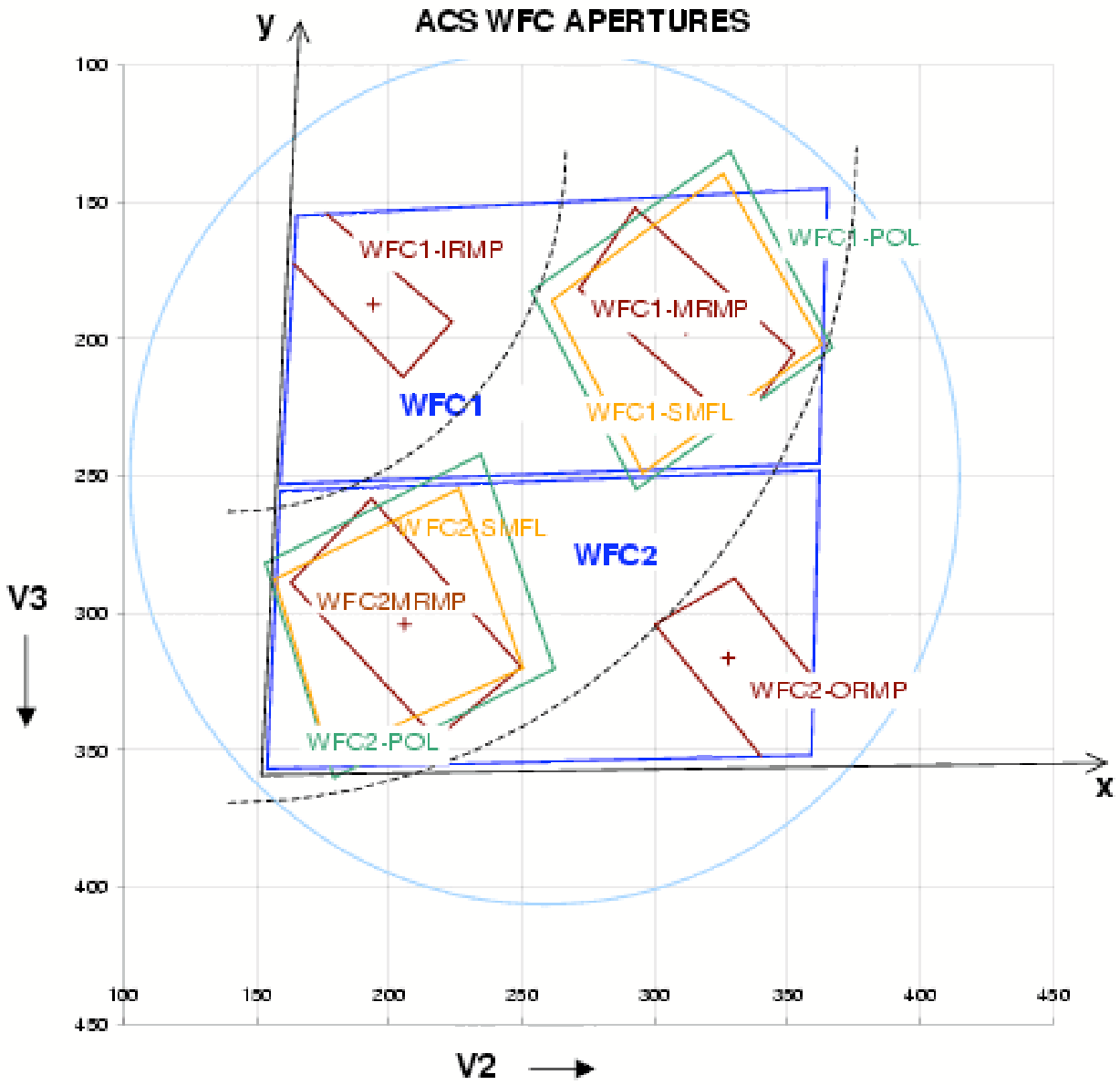

Fig. 11.— The locations of ramp apertures on the WFC detectors as shown in Figure 7.4 from the ACS Instrument Handbook. With the exception of FR782N and FR931N all of the ramps tested on the WFC used WFC1 apertures.